

Ab initio study of gap opening and screening effects in gated bilayer graphene

Paola Gava, Michele Lazzeri, A. Marco Saitta, and Francesco Mauri

IMPMC, CNRS, IPGP, Universités Paris 6 et 7, 140 Rue de Lourmel, 75015 Paris, France
(Dated: October 31, 2018)

The electronic properties of doped bilayer graphene in presence of bottom and top gates have been studied and characterized by means of density-functional theory (DFT) calculations. Varying independently the bottom and top gates it is possible to control separately the total doping charge on the sample and the average external electric field acting on the bilayer. We show that, at fixed doping level, the band-gap at the K point in the Brillouin zone depends linearly on the average electric field, whereas the corresponding proportionality coefficient has a nonmonotonic dependence on doping. We find that the DFT-calculated band-gap at K , for small doping levels, is roughly half of the band-gap obtained with standard tight binding (TB) approach. We show that this discrepancy arises from an underestimate, in the TB model, of the screening of the system to the external electric field. In particular, on the basis of our DFT results we observe that, when bilayer graphene is in presence of an external electric field, both interlayer and intralayer screenings occur. Only the interlayer screening is included in TB calculations, while both screenings are fundamental for the description of the band-gap opening. We finally provide a general scheme to obtain the full band structure of gated bilayer graphene for an arbitrary value of the external electric field and of doping.

PACS numbers: 71.15.Mb, 73.22.-f, 73.61.-r, 81.05.Uw

I. INTRODUCTION

Among the nanoscale forms of carbon, bilayer graphene has recently attracted much interest.^{1,2,3,4,5,6,7,8} Indeed, it has been found, both theoretically and experimentally, that in presence of an asymmetry between the two graphene layers, generated by an external electric field, a band-gap can be opened. This makes bilayer graphene a tunable-gap semiconductor and therefore an exciting structure for future application in nanoelectronics.

In particular, in the experiments of Ohta et al.³ bilayer graphene is synthesized on silicon carbide (SiC) substrate, and a small n -type doping is acquired by the system from the substrate. In this case, the bilayer symmetry is broken by the dipole field created by the depletion of charge on SiC and accumulation of charge on the bilayer. Additional n doping is induced by deposition of potassium atoms above the bilayer. Varying the concentration of potassium atoms, one can vary the asymmetry between the two sides of the system and measure the electronic properties and the band-gap opening by angle-resolved photoemission spectroscopy (ARPES).

Oostinga et al.⁴ used a double-gated system, where monolayer and bilayer graphenes are placed between two dielectrics, which act as bottom and top gates. The double-gated structure gives the possibility to control independently the doping level and the perpendicular electric field acting on the system. In this configuration, they measure the dependence of the resistance on the temperature and on the electric field. They observe a gate-induced insulating state in bilayer graphene which originates from the band-gap opening between the valence and conduction bands.

As for theoretical studies, McCann⁵ used a tight binding (TB) model to study the band structure of the bilayer graphene in presence of an energy difference between the two layers, which determines a band-gap opening. In particular, he considered a single gate acting on the system, and he found a roughly linear relation of the gap with the accumulated charge n on the bilayer, for n values up to $10 \times 10^{12} \text{cm}^{-2}$. Min et al.⁶ performed ab initio density-functional theory (DFT) calculations of undoped bilayer graphene in a constant external electric field, using the generalized gradient approximation (GGA) for the exchange-correlation functional. They confirmed the general picture provided by the TB model, although DFT screening results stronger. Moreover, Aoki et Amawashi⁹ performed an ab initio DFT study on the band structure dependence of undoped layered graphene on the stacking and external field, using the local density approximation (LDA) for the exchange-correlation functional. In contrast with the GGA study of Min et al.,⁶ their results on undoped bilayer graphene in a uniform external electric field are in agreement with the TB ones. Again, Castro et al.^{7,8} showed experimentally, by measuring the Hall conductivity and the cyclotron mass of biased bilayer graphene, and theoretically, using TB methods, that a band-gap between the valence and conduction bands can be tuned by an applied electric field.

Other theoretical DFT studies have been devoted to the understanding of the band structure dependence on the stacking geometry,¹⁰ on the presence of adsorbed molecules,¹¹ and to the analysis of the distribution of the induced charge densities.¹² Instead, other experimental studies focused on the Raman spectra of bilayer graphene.^{13,14,15,16} Recently, an experimental work on infrared spectra of gated bilayer graphene as a function of doping appeared,¹⁷ and a comparison with TB calcula-

tions suggests that the TB prediction of the gate-induced band-gap is overestimated.

In this work, we study by means of DFT ab initio calculations the band-gap opening in bilayer graphene, both as a function of the external electric field and as a function of doping. The paper is organized as follows: in Sec. II a description of the system we investigate is reported, along with the computational details. Results are presented in Sec. III, where the dependence of the gap on the electric field and doping is first shown and compared with TB calculations. Then, a detailed analysis of the screening properties of the bilayer to the external electric field is reported. The effect of the electronic temperature on the screening is also investigated, and the nonmonotonic behavior of the band-gap as a function of doping at fixed electric field is explained. The *GW* correction of the DFT-calculated response of the gap to the external electric field is presented. Finally, a general scheme to obtain the full band structure of gated bilayer graphene is provided, and a comparison with experimental findings is reported. In Sec. IV our conclusions are drawn. In the Appendix we describe in detail the top and bottom gates implementation in our DFT calculations.

II. THEORETICAL BACKGROUND

A. Bilayer graphene in bottom and top gates

The experimental setup where bilayer graphene feels different bottom and top gates is schematically represented in Fig.1. The bilayer is first grown on a dielectric material, of width D_2 and relative dielectric constant ϵ_{r2} . Applying a voltage difference V_{g2} (bottom gate) between the dielectric and the bilayer, a doping charge per unit surface $n_2e = \xi_2 V_{g2}$ is accumulated on the bilayer, where e is the electron charge ($e = -|e|$) and $\xi_2 = \epsilon_0 \epsilon_{r2} / D_2$. ϵ_0 is the permittivity of the vacuum. Depositing another dielectric material of width D_1 and with relative dielectric constant ϵ_{r1} over the bilayer, and applying a gate voltage V_{g1} (top gate) between the dielectric and the bilayer, an additional doping charge per unit surface $n_1e = \xi_1 V_{g1}$ is accumulated, where $\xi_1 = \epsilon_0 \epsilon_{r1} / D_1$. A total doping charge ne is therefore accumulated on the bilayer, where $n = n_1 + n_2$. According to standard notation, positive n corresponds to electron doping and negative n corresponds to hole doping. ρ_1 and ρ_2 are the electronic charges per unit area (with respect to the neutral case) accumulated on layer 1 and layer 2, respectively. In particular, the sum of ρ_1 and ρ_2 is determined by the electrostatics, and it is equal to the sum of n_1 and n_2 . However, the individual values of ρ_1 and ρ_2 depend on the screening properties of the system, and in general $\rho_1 \neq n_1$ and $\rho_2 \neq n_2$. In the configuration shown in Fig.1, layer 1 and layer 2 of the bilayer feel an electric field E_1 and E_2 , respectively, given by

$$E_1 = -n_1 e / \epsilon_0, \quad (1)$$

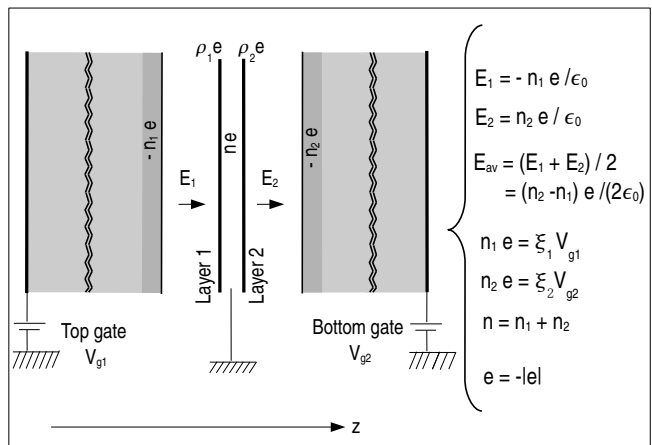


FIG. 1: Schematic representation of the experimental setup where bilayer graphene is placed between two dielectric materials, and it is doped by applying bottom (V_{g2}) and top (V_{g1}) gates. The width of the two dielectrics is much larger than the distance between the dielectrics and the bilayer. A doping charge per unit area $ne = (n_1 + n_2)e$ is accumulated on the bilayer, where $n_2e = \xi_2 V_{g2}$ and $n_1e = \xi_1 V_{g1}$ are the charges from bottom and top gates, respectively. ρ_1e and ρ_2e are the electronic charges per unit area (with respect to the neutral case) on layer 1 and layer 2, respectively. In particular, $(\rho_1 + \rho_2)e = (n_1 + n_2)e$, while $\rho_1 \neq n_1$ and $\rho_2 \neq n_2$. Layer 1 and layer 2 of bilayer feel electric fields $E_1 = -n_1e/\epsilon_0$ and $E_2 = n_2e/\epsilon_0$, which determine an average electric field $E_{av} = (n_2 - n_1)e/(2\epsilon_0)$. ϵ_0 is the permittivity of the vacuum.

$$E_2 = n_2 e / \epsilon_0. \quad (2)$$

The average electric field E_{av} is defined as

$$\begin{aligned} E_{av} &= (E_1 + E_2) / 2 \\ &= (n_2 - n_1) e / (2\epsilon_0) \\ &= (n_1 - n_2) |e| / (2\epsilon_0). \end{aligned} \quad (3)$$

Positive E_{av} is oriented from dielectric 1 to dielectric 2 (*i.e.*, from top to bottom gate). When n_1 and n_2 are equal, we are in the case of equal bottom and top gates, and E_{av} vanishes. When n_1 is zero, we are in presence of bottom gate alone. The top gate can also be generated by a chemical doping, with the deposition of alkali or halogen atoms on the bilayer. In this work, the electric fields E_1 and E_2 are simulated using periodically repeated boundary conditions by introducing dipole and monopole potentials, as described in the Appendix.

The presence of different bottom and top gates generates an electrostatic potential which is different on layer 1 with respect to layer 2, and this asymmetry gives origin to a band-gap opening. In Fig.2 we show the band structure of undoped bilayer graphene, in absence of bottom and top gates, where no gap is observed, and in presence of different bottom and top gates in which case a gap is opened. In order to simplify the discussion, in this work we define a signed gap U at the K point in the Brillouin zone (BZ), which is negative for $E_{av} < 0$, and positive for $E_{av} > 0$.

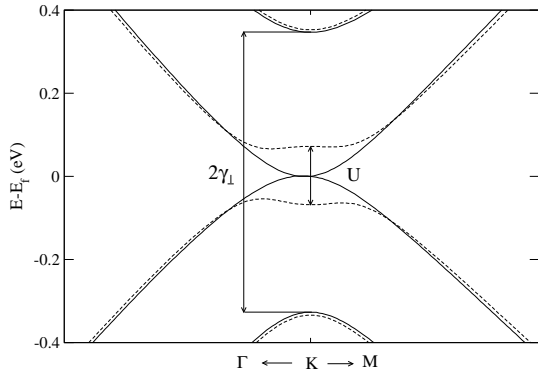


FIG. 2: Band structure, around the K point in the BZ, of undoped bilayer graphene in absence of bottom and top gates (solid line) and in presence of different bottom and top gates (dashed line).

B. Computational details

The presented ab initio results based on the DFT, are done using both the Perdew-Burke-Ernzerhof (PBE) (Ref.¹⁸) GGA, and the Perdew-Zunger (PZ) Ref.⁽¹⁹⁾ LDA exchange-correlation functionals. Core electrons are taken into account using the pseudopotential method, with norm-conserving Troullier-Martin pseudopotentials.²⁰ Plane-waves basis set is used to describe valence electron wave functions and density, up to a kinetic energy cut-off of 40 and 600 Ry, respectively. The electronic eigenstates have been occupied with a Fermi-Dirac distribution, using an electronic temperature of 300 and 30 K. The BZ integration has been performed with a uniform \mathbf{k} point grid of $(80 \times 80 \times 1)$ and $(240 \times 240 \times 1)$ for the two temperatures, respectively. The experimental lattice constant $a = 2.46 \text{ \AA}$ of two-dimensional graphite is used. The layer-layer distance d is fixed at the value of 3.35 \AA , as in graphite. The two layers are arranged according to Bernal stacking. The length L of the supercell along z is 17.2 \AA . Calculations have been performed using the PWscf code²¹ of the Quantum ESPRESSO distribution²².

In this work we perform also TB calculations. The TB model we use is characterized by two parameters, γ_{\parallel} and γ_{\perp} , which represent the first nearest-neighbors in-plane hopping and the interplane hopping between vertically superposed atoms in the Bernal stacking configuration, respectively. γ_{\parallel} is related to the Fermi velocity in single layer graphene, $v_f = \gamma_{\parallel} a \sqrt{3} / (2\hbar)$. We use a value of $\gamma_{\parallel} = 3.1 \text{ eV}$, as inferred from experimental measurements.^{3,13,23} Within the TB model, $2\gamma_{\perp}$ corresponds to the band splitting between the lowest occupied π band and the highest unoccupied π band at K (see Fig.2). We use a value of $\gamma_{\perp} = 0.4 \text{ eV}$, as obtained from experimental measurements.^{3,13,17} Similar values for these TB

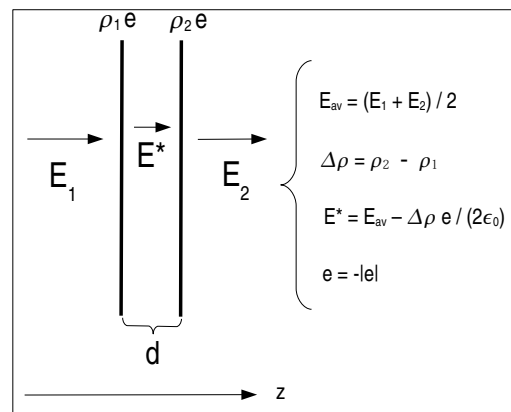


FIG. 3: Schematic representation of the electrostatic model used with TB calculations. The bilayer of thickness d feels an external electric field E_1 on layer 1 and E_2 on layer 2, which induce a charge per unit surface $\rho_1 e$ and $\rho_2 e$ on layer 1 and layer 2 and a local electric field E^* .

parameters have been used in literature.^{5,7,8} In addition to these parameters, we consider the energy difference between layer 2 and layer 1 induced by the electric field, which coincides with the signed gap U at the K point in the BZ (see Fig.2 and Ref.³).

In the TB formalism, in order to obtain the relation between the gap U and the average electric field E_{av} , a simple electrostatic model is used. In Fig.3 we show a schematic representation of this electrostatic model. Charges per unit surfaces $\rho_1 e$ and $\rho_2 e$ are concentrated on the two layers of the bilayer, which create a screened field E^* inside the system. Using simple electrostatic equations, we have

$$E^* = E_{av} - \frac{\Delta\rho e}{2\epsilon_0}, \quad (4)$$

where $E_{av} = (E_1 + E_2)/2$ and $\Delta\rho = \rho_2 - \rho_1$. $\Delta\rho$ is calculated from the square modulus of the eigenfunctions in the two layers. The energy difference between layer 2 and layer 1, *i.e.*, the band-gap U at K , is given by

$$U = -d E^* e. \quad (5)$$

Inserting into eq.(5) the expression of E^* as given in eq.(4), and writing E_1 and E_2 as in Eq.(1) and (2), we obtain:

$$U = \frac{de^2}{2\epsilon_0} (n_1 - n_2 + \Delta\rho). \quad (6)$$

Therefore, in the TB calculations the electronic screening is evaluated using the simplified electrostatic model described above, contrary to the DFT formalism where the detailed shape of the charge distribution is fully taken into account.

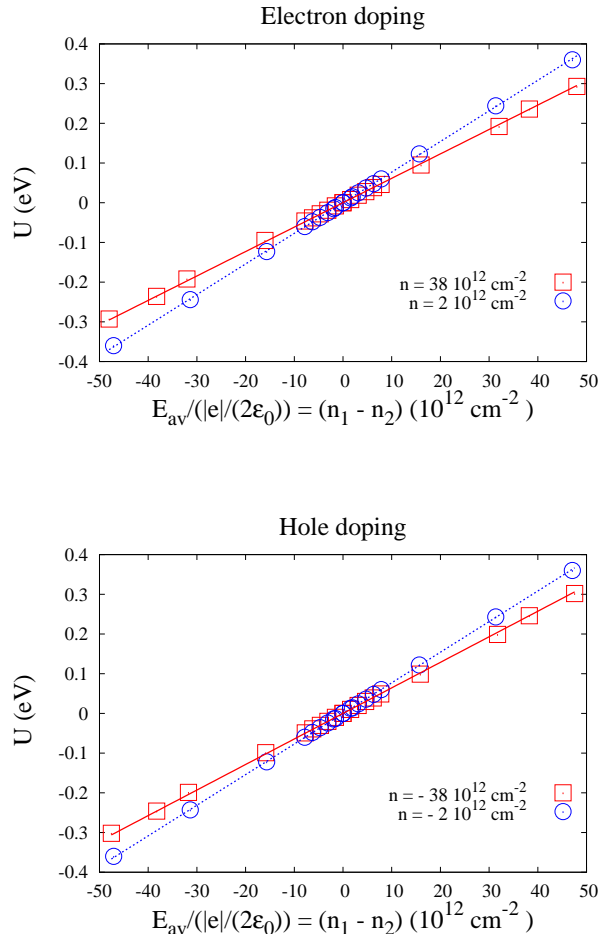


FIG. 4: (Color online) DFT-GGA calculated U as a function of $(n_1 - n_2)$, *i.e.*, the average electric field divided by $|e|/(2\epsilon_0)$, for electron and hole dopings. Two values of electron doping are shown, $n = 38$ and $2 \times 10^{12} \text{ cm}^{-2}$, and two values of hole doping, $n = -38$ and $-2 \times 10^{12} \text{ cm}^{-2}$. Points are the calculated values, for an electronic temperature of 300 K, while lines are linear fits.

III. RESULTS

A. Band gap as a function of the external electric field and doping charge

As anticipated in Sec.II A, when bilayer graphene feels different bottom and top gates, a band-gap U is opened. In this section we first investigate the dependence of U on the average external electric field E_{av} , at fixed doping n .

In Fig.4 we show the DFT-GGA calculated U as a function of $(n_1 - n_2)$ [*i.e.*, the average electric field E_{av} divided by $|e|/(2\epsilon_0)$], for two values of electron and hole dopings. These values of doping are chosen as representative of two different doping regimes, which can be

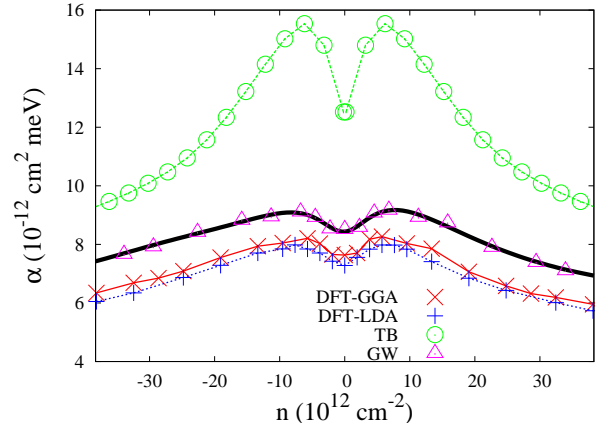


FIG. 5: (Color online) α as a function of doping n , for an electronic temperature of 300 K, calculated with DFT-GGA (\times crosses) and LDA ($+$ crosses), calculated using TB model with $\gamma_{\parallel} = 3.1 \text{ eV}$ and $\gamma_{\perp} = 0.4 \text{ eV}$ (circles), and using *GW* correction (up-triangles). The *GW* correction is obtained as described in Sec. III E. The continuous thick (black) line is the fit, as written in Eq.(33), of the *GW* result. The value of α in absence of electronic screening is independent of the doping, and it is $\alpha^{\text{bare}} = de^2/(2\epsilon_0) = 30.3 \times 10^{-12} \text{ cm}^2 \text{ meV}$.

experimentally obtained in bilayer graphene by the application of a gate voltage with a SiO_2 dielectric¹⁴ or with a polymeric electrolyte.¹⁵ Our results show that U has a linear dependence on the applied electric field E_{av} . We therefore define a linear response $\alpha(n)$ such that

$$U(n, E_{av}) = \alpha(n)(n_1 - n_2). \quad (7)$$

In Fig.5 we show α as a function of doping n , calculated from Eq.(7), for an electronic temperature of 300 K, within the DFT-GGA and LDA functionals, and using the TB model described in Sec.II B. Contrary to previous results in literature,^{6,9} our LDA and GGA results are very similar, and not in agreement with the TB ones. In particular, our results for zero doping and GGA functional are in agreement with the previous GGA study.⁶ They disagree instead with the ones computed with LDA functional in Ref.⁹. This is probably due to the fact that in Ref.⁹ the authors used a coarse \mathbf{k} point sampling ($10 \times 10 \times 1$) with respect to the ones used in this work and in Ref.⁶, and their results are likely unconverged. In the following we only present our GGA results. Both DFT and TB α 's display a nonmonotonic behavior as a function of doping. However, the values of the DFT-calculated α are substantially different from the TB ones, especially for low doping values, *i.e.*, when the Fermi level is close to the band-gap edges. This is the most interesting case for the application of the bilayer as active device in electronics.

We notice that in the absence of electronic screening,

α is independent of the doping, and it is

$$\alpha^{\text{bare}} = \frac{de^2}{2\epsilon_0} = 30.3 \times 10^{-12} \text{cm}^2 \text{meV}. \quad (8)$$

Thus, with the inclusion of the electronic screening, the DFT-calculated α becomes roughly three times smaller than the α^{bare} , which suggests that the screening effects are crucial for the description of the band-gap.

In order to understand the origin of the difference between the DFT and TB results, we notice that this can be due (i) to the calculated electronic band structure and charge transfer and (ii) to the electrostatic model used in the TB calculations, which gives a simplified description of the crucial screening effects, fully included in the DFT formalism. To verify the quality of the electrostatic model, we introduce the quantity $\eta(n)$ defined as:

$$\Delta\rho(n, U) = \eta(n)U. \quad (9)$$

$\Delta\rho = \rho_2 - \rho_1$ is calculated from

$$\rho_2 = \int_0^\infty [\rho(z) - \rho_0(z)] dz, \quad (10)$$

$$\rho_1 = \int_{-\infty}^0 [\rho(z) - \rho_0(z)] dz, \quad (11)$$

where $\rho(z)$ is the planar average of the electronic charge density (per unit volume) for a doping n and in presence of E_{av} and $\rho_0(z)$ is the planar average of the electronic charge density (per unit volume) for the neutral case, with $E_{\text{av}}=0$. Here and in the following $z=0$ indicates the plane at the midpoint of the two graphene layers. In our DFT calculations, $\pm\infty$ corresponds to $\pm L/2$, where L is the length of the supercell along z .

η is a measure of the charge transfer between layers in the presence of a band-gap U . We introduce this quantity because it is a direct outcome of the TB calculations, and no further electrostatic model is needed to compute it. Moreover, according to the electrostatic model used together with the TB formalism, described in Sec. IIB, the relation which gives α as a function of η is obtained dividing Eq.(6) by U ,

$$\alpha(n) = \frac{\alpha^{\text{bare}}}{1 - \eta(n) \alpha^{\text{bare}}}. \quad (12)$$

In Fig.6 we show $\eta(n)$, calculated from Eq.(9), for an electronic temperature of 300 K, within the DFT and using the TB model described in Sec.IIB. η as a function of n has a nonmonotonic behavior as found for $\alpha(n)$, and this trend is well described by the two methods. However, the values of η calculated with the two formalisms are different. Since no electrostatic model is used in the TB calculations, we conclude that this discrepancy originates only from the difference between the DFT- and TB-calculated band structure and charge transfer.

Moreover, comparing the DFT and TB results of $\alpha(n)$ and $\eta(n)$, we see that, for low doping levels, the relative

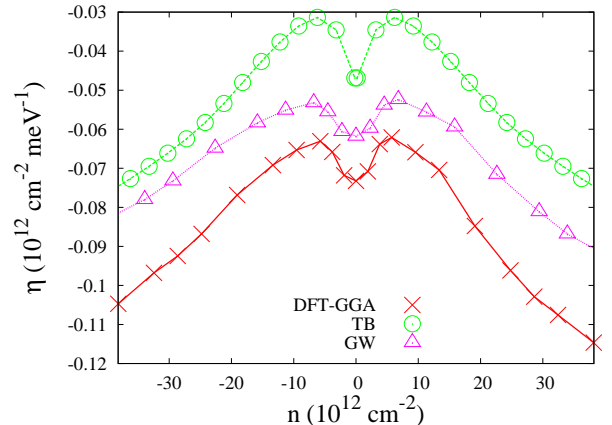


FIG. 6: (Color online) η as a function of doping n , calculated with DFT-GGA (crosses), with TB model (circles), and with GW correction (up-triangles), for an electronic temperature of 300 K. The GW correction is obtained as described in Sec. III E.

difference, with respect to DFT values, of the TB/DFT $\alpha(n)$'s is around 60%, while the analogous difference for η is around 30%. Therefore, the electrostatic model used to compute $\alpha(n)$ in the TB formalism introduces a large error in the description of the band-gap opening in presence of an external electric field.

B. Electronic screening effects

In this section we analyze where the simplified electrostatic model used in the TB calculations fails, and we propose a more sophisticated one. First of all, we know that in the TB formalism the energy difference between the two layers coincides with the band-gap U at the K point in the BZ. In Fig.7 we show the band-gap U as a function of $V_{2-1} = V_2 - V_1$, where V_2 and V_1 are the planar average of the DFT-calculated ionic, Hartree, and electrostatic potential energy on layer 2 and layer 1, respectively. The inclusion of the exchange-correlation potential does not change the result. We can notice that even in DFT formalism, U is correlated with the potential energy difference between the two layers, and in particular,

$$U = \beta V_{2-1}, \quad (13)$$

where $\beta = 1.072$, slightly higher than the expected unitary slope.

To better understand the screening effects in the system, we investigate the linearly induced charge (per unit volume) $\rho^{(1)}$

$$\rho^{(1)}(z; n, E_{\text{av}}) = \frac{\partial \rho(z; n, E_{\text{av}})}{\partial E_{\text{av}}} E_{\text{av}} \quad (14)$$

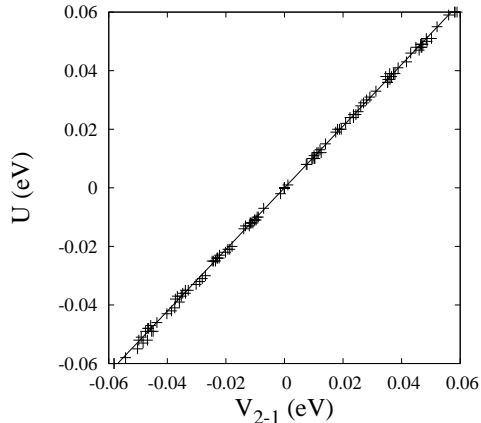


FIG. 7: DFT-GGA calculated U as a function of the difference between the planar average of the ionic, Hartree, and electrostatic potential energy on layer 2 and layer 1, V_{2-1} , for different values of doping and of E_{av} . Points are the calculated values; the line is the linear fit, $U = 1.072 \times V_{2-1}$.

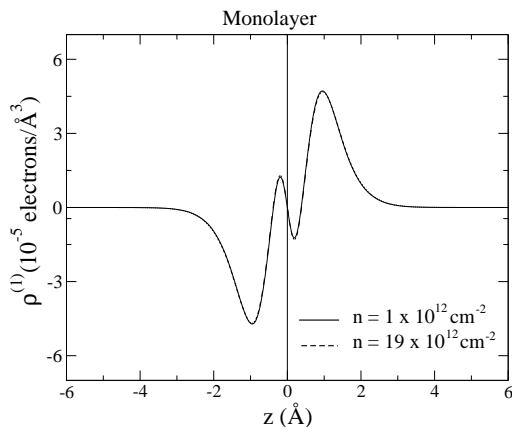


FIG. 8: Planar average of the linear induced charge (per unit volume) $\rho^{(1)}$ of a graphene monolayer in presence of an external electric field $E_{av} = 1.6 \times e/(2\epsilon_0) 10^{12} \text{cm}^{-2}$ for a doping level $n = 1 \times 10^{12} \text{cm}^{-2}$ (continuous line) and $n = 19 \times 10^{12} \text{cm}^{-2}$ (dashed line).

$$\simeq \frac{1}{2} [\rho(z; n, E_{av}) - \rho(z; n, -E_{av})], \quad (15)$$

where $\rho(z; n, E_{av})$ is the planar average of the charge density (per unit volume) at a given doping level n and in presence of an external average electric field E_{av} . Such $\rho^{(1)}$ is antisymmetric with respect to $z=0$, *i.e.*, $\rho^{(1)}(z; n, E_{av}) = -\rho^{(1)}(-z; n, E_{av})$. In our plots we use the finite difference expression of $\rho^{(1)}$, *i.e.*, Eq.(15).

In Fig.8 we show $\rho^{(1)}$ for the graphene monolayer in presence of an external electric field $E_{av} = 1.6 \times e/(2\epsilon_0) 10^{12} \text{cm}^{-2}$ for two different doping levels. In this case, ob-

viously no charge transfer between layers occurs, and the electronic screening to the external electric field is only characterized by an intralayer polarization. Moreover, we notice that the dependence of the induced charge on the doping is negligible.

In Fig.9-a) we show $\rho^{(1)}$ for bilayer graphene in presence of the same external electric field. First of all, we notice that $\rho^{(1)}$ in the monolayer and in the bilayer are of the same order of magnitude. Then, we observe that the electronic screening of the bilayer to the external electric field, is characterized by (i) a charge transfer between the two layers, which is peculiar to the bilayer and (ii) an intralayer polarization, which is also present in the monolayer.

In order to separate in the bilayer the interlayer from the intralayer polarization, we notice from Fig.8 that the intralayer induced charge is antisymmetric with respect to each individual layer. Thus we decompose the induced charge in the bilayer into a symmetric component, $\rho_s^{(1)}$, and an antisymmetric component, $\rho_a^{(1)}$, with respect to each individual layer. $\rho_s^{(1)}$ and $\rho_a^{(1)}$ are defined for $z \in \{-d; d\}$, *i.e.*, in an interval of width d around each layer, where d is the intralayer distance; they are calculated as

$$\rho_{s/a}^{(1)}(z) = \frac{1}{2} \left\{ \rho^{(1)}(z) \pm \rho^{(1)}[\text{sign}(z) d - z] \right\}. \quad (16)$$

The symmetric, $\rho_s^{(1)}$, and antisymmetric, $\rho_a^{(1)}$, components are related to the charge transfer between the two layers and to the intralayer polarization, respectively.

In Fig.9-b) we show the symmetric component $\rho_s^{(1)}$, with respect to each layer, of the induced charge $\rho^{(1)}$ shown in Fig.9-a). In Fig.9-c) we show the antisymmetric component $\rho_a^{(1)}$. In particular, $\rho_a^{(1)}$ is very similar to the induced charge in the monolayer (Fig.8), and it is of the same order of magnitude of the total induced charge in the bilayer [Fig.9-a). On the basis of this qualitative analysis of the linearly induced charge, we conclude that the intralayer polarization, which is not taken into account in the TB formalism, gives an important contribution to the screening properties of the system.

In order to quantify the effect of the induced charge on the gap, we write the exact expression of the potential energy difference V_{2-1} in terms of the linearly induced charge $\rho^{(1)}$ and of the external average electric field E_{av} using the Poisson equation in one dimension. We obtain the following:

$$\begin{aligned} V_{2-1} &= V(d/2) - V(-d/2) = -de E_{av} + \\ &- \frac{e^2}{2\epsilon_0} \int_{-\infty}^{+\infty} \left| \frac{d}{2} - z \right| \rho^{(1)}(z) dz + \\ &+ \frac{e^2}{2\epsilon_0} \int_{-\infty}^{+\infty} \left| -\frac{d}{2} - z \right| \rho^{(1)}(z) dz, \end{aligned} \quad (17)$$

where $\pm d/2 = \pm 1.675 \text{ \AA}$ is the z coordinate of the two layers. Considering that $\rho^{(1)}(z) = -\rho^{(1)}(-z)$, by simple

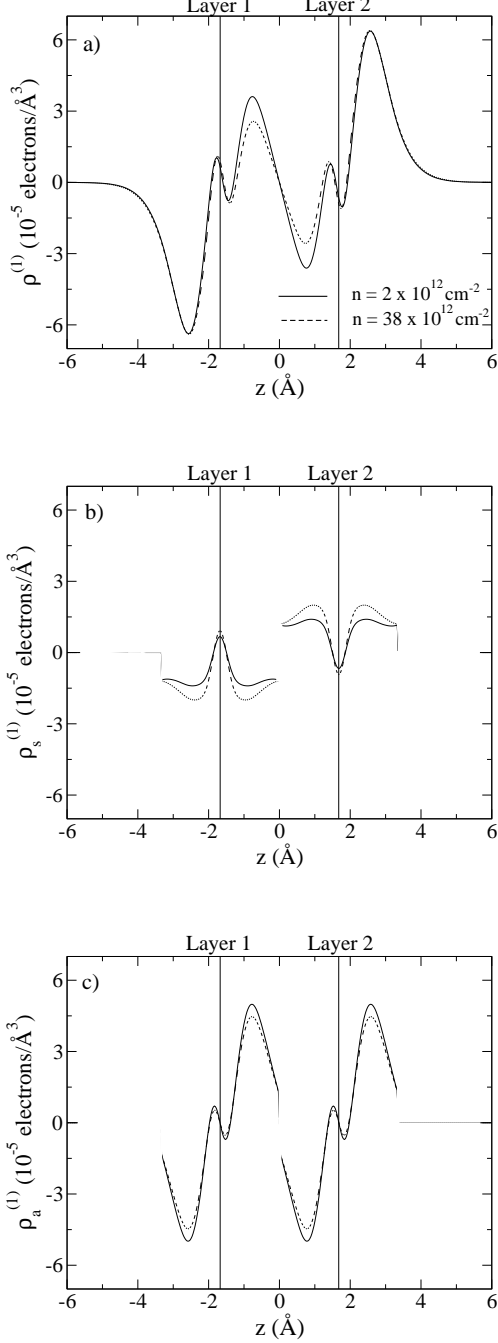


FIG. 9: a) Planar average of the linearly induced charge (per unit volume) $\rho^{(1)}$ for bilayer graphene in presence of an external electric field $E_{av} = 1.6 \times e/(2\epsilon_0) 10^{12}\text{cm}^{-2}$ for a doping level $n = 2 \times 10^{12}\text{cm}^{-2}$ (continuous line) and $n = 38 \times 10^{12}\text{cm}^{-2}$ (dashed line); b) symmetric component, $\rho_s^{(1)}$; and c) antisymmetric component, $\rho_a^{(1)}$, with respect to each layer, of the linearly induced charge $\rho^{(1)}$ shown in a) for the same doping levels.

algebra and without approximations we can rewrite V_{2-1}

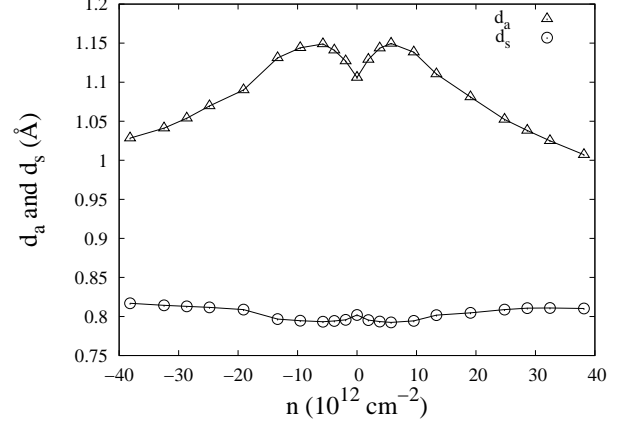


FIG. 10: d_a and d_s as a function of doping n , as defined in Eqs.(22) and (23).

as

$$V_{2-1} = -ed E_{av} + \frac{de^2}{2\epsilon_0} \Delta\rho + e D_a - e D_s, \quad (18)$$

where

$$D_a = \frac{e}{\epsilon_0} \int_0^d (z - \frac{d}{2}) \rho_a^{(1)}(z) dz, \quad (19)$$

$$D_s = \frac{e}{\epsilon_0} \int_0^d |z - \frac{d}{2}| \rho_s^{(1)}(z) dz, \quad (20)$$

and

$$\Delta\rho = \int_0^\infty \rho^{(1)}(z) dz - \int_{-\infty}^0 \rho^{(1)}(z) dz. \quad (21)$$

D_a and D_s represent the contributions to the potential energy difference V_{2-1} given by the antisymmetric and symmetric components of the linearly induced charge around each layer. Equation (18) gives the exact expression of V_{2-1} as a function of the external electric field and of the screening charge.

We now rewrite D_a and D_s as follows:

$$D_a = d_a(n) E_{av}, \quad (22)$$

$$D_s = \frac{e}{2\epsilon_0} d_s(n) \Delta\rho, \quad (23)$$

where D_a has a linear dependence on the average electric field through a proportionality constant d_a which depends on the doping n . D_s is instead the contribution to the interlayer polarization coming from the width of the transferred charge. Therefore we write it in a form consistent with the other interlayer term in Eq.(18), *i.e.*, $de^2/(2\epsilon_0)\Delta\rho$, with a proportionality constant d_s which depends on the doping n .

In Fig.10 we show d_a and d_s as a function of doping n . Since d_s is almost independent of the doping and

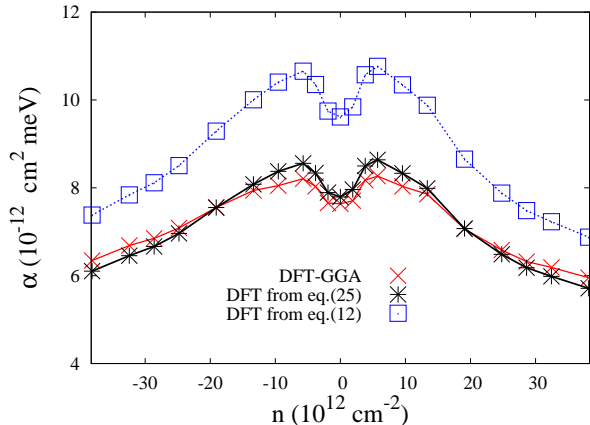


FIG. 11: (Color online) $\alpha(n)$ calculated with DFT-GGA (\times crosses) from Eq.(12) using the DFT-GGA calculated $\eta(n)$ (squares) and from Eq.(25) using the DFT-GGA calculated $\eta(n)$ (stars).

d_a has a variation in the order of 5%, we replace them with their average values calculated on the doping range considered, $\bar{d}_a=1.09$ Å, and $\bar{d}_s=0.80$ Å. Using only this approximation and Eq.(13), we have

$$U = \beta \left[-e(d - \bar{d}_a)E_{av} + \frac{e^2}{2\epsilon_0}(d - \bar{d}_s)\Delta\rho \right]. \quad (24)$$

We notice that the simplified electrostatic model described in Sec.IIB, *i.e.*, Eq.(6), used in TB calculations, is equivalent to consider, in Eq.(24), $\beta = 1$, $\bar{d}_a = 0$ (*i.e.* $\rho_a^{(1)}(z) = 0$), and $\bar{d}_s = 0$ [*i.e.*, $\rho_s^{(1)}(z) = \delta(|z| - d/2) \Delta\rho/2 \text{ sign}(z)$].

Considering Eq.(24), and the definition of α [as in Eq.(7)] and η [as in Eq.(9)] we obtain another relation between α and η as follows:

$$\alpha(n) = \frac{\alpha^{\text{bare}}\beta (d - \bar{d}_a)/d}{1 - \eta(n) \alpha^{\text{bare}}\beta (d - \bar{d}_s)/d}. \quad (25)$$

Equation (25) gives the approximate relation between U , the average electric field, the screening charge obtained considering the intralayer polarization, and considering the width of the transferred charge between layers. This equation substitutes Eq.(12) which comes from the simplified electrostatic model described in Sec.IIB.

In Fig.11 we show the DFT-calculated $\alpha(n)$, $\alpha(n)$ obtained from Eq.(12) using the DFT-calculated $\eta(n)$, and from the electrostatic model of Eq.(25) using the DFT-calculated $\eta(n)$. One can see that the simplified electrostatic model is not able to describe the DFT results. Instead, $\alpha(n)$ obtained from the model of Eq.(25) is able to correctly reproduce the DFT calculations.

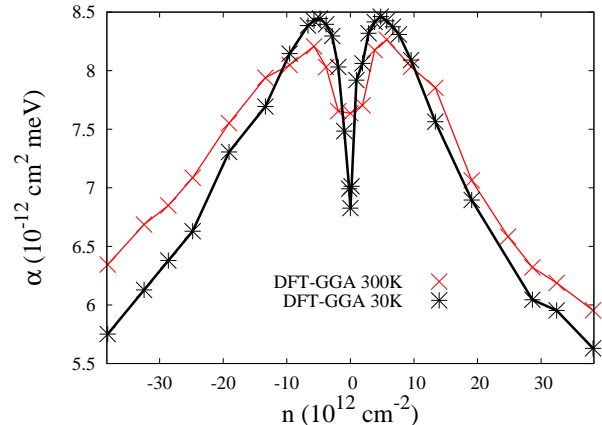


FIG. 12: (Color online) The DFT-GGA calculated α as a function of the doping n for an electronic temperature of 300 (crosses) and 30 K (stars).

C. Effect of the electronic temperature on α as a function of doping n

In Sec. IIIA we have shown that in the bilayer the electronic screening to the external electric field is crucial for a correct evaluation of the band-gap. At low doping level the screening is expected to depend on the broadening parameter, and in this section we investigate the effect of the electronic temperature on the screening and on α .

In Fig.12 we show the DFT-calculated α as a function of n for an electronic temperature of 300 and 30 K. The variation in screening with the broadening parameter depends on the doping n . Since the doping levels which are interesting for applications of the bilayer as active device in nanoelectronics are small values around the zero doping, we focus on this doping range.

In Fig.13 we show the DFT-calculated α as a function of the electronic temperature T for electron doping values between 0 and $5.72 \times 10^{12} \text{cm}^{-2}$. In this range of doping, we can see that the difference between α at 300 and 30 K is largest for zero doping. In particular, for zero doping the band-gap at 30 K results to be about 10% smaller than at 300 K.

D. Nonmonotonic behavior of α as a function of doping n

As shown in Figs.5 and 6, both DFT-calculated α and η have a nonmonotonic behavior as a function of the doping n . α and η represent the linear response of U to the external average electric field E_{av} and the linear response of $\Delta\rho$ to the band-gap U , respectively. Up to now, we calculated α and η for finite values of E_{av} and U . In this section we show that perturbation theory (PT)

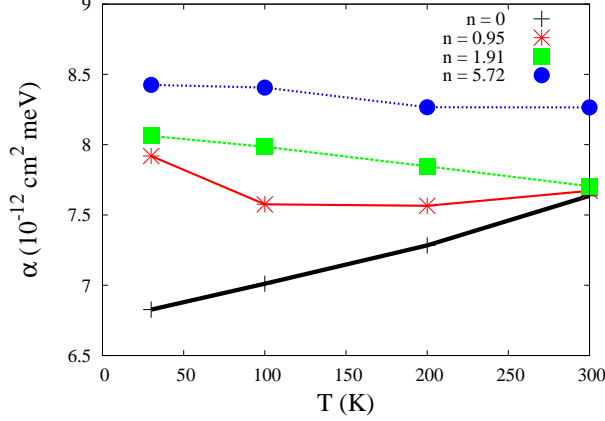


FIG. 13: (Color online) The DFT-GGA calculated α as a function of the electronic temperature T , for small values of electron doping. The values of doping n are in units of 10^{12}cm^{-2} .

explains the origin of this nonmonotonic behavior as a function of doping n .

For the numerical evaluation of the expressions obtained from PT, we use the band structure calculated with the TB model. Indeed, even if TB results for α and η differ from the DFT ones, TB is able to catch the nonmonotonic trend of these quantities as a function of the doping n . Moreover, we limit our PT calculations to $\eta(n)$. Indeed, since the relation between η and α is monotonic [see Eq.(25)], the nonmonotonic behavior of η is able to explain also the nonmonotonic behavior of α as a function of n .

In order to calculate $\eta(n)$ with PT, we consider $\hat{H}_{\mathbf{k}}^{(0)}$, which is the unperturbed TB Hamiltonian. $\hat{H}_{\mathbf{k}}^{(0)}$ is a 4×4 matrix which depends on the wave vector \mathbf{k} and is written on the basis of $2p_z$ orbitals centered on the four atoms of the unit-cell, ordered as A, B, A', B' (A and B are the two carbon atoms on layer 1, A' and B' are the two carbon atoms on layer 2, and in the Bernal stacking configuration A and A' are vertically superposed). In presence of a band splitting U (see Fig.2), the Hamiltonian $\hat{H}_{\mathbf{k}}$ can be written as

$$\hat{H}_{\mathbf{k}} = \hat{H}_{\mathbf{k}}^{(0)} + \frac{U}{2} \hat{\Delta}\rho, \quad (26)$$

where

$$\hat{\Delta}\rho = \begin{pmatrix} 1 & 0 & 0 & 0 \\ 0 & 1 & 0 & 0 \\ 0 & 0 & -1 & 0 \\ 0 & 0 & 0 & -1 \end{pmatrix}. \quad (27)$$

Using first-order PT, we obtain the following expression for $\eta = \left(\frac{d\Delta\rho}{dU} \right)$:

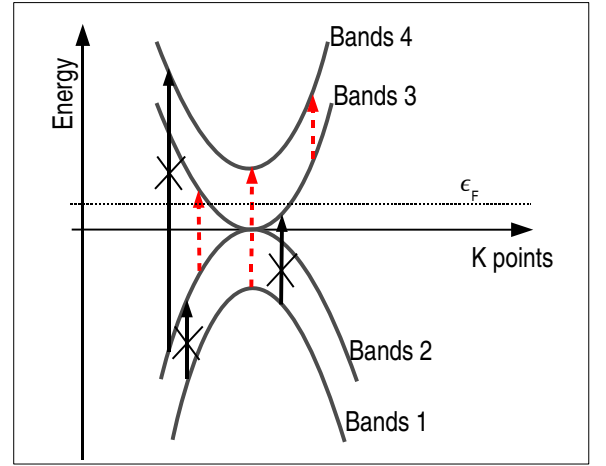


FIG. 14: (Color online) Schematic representation of allowed (dashed arrows) and not allowed (continuous arrows) contributions from band-to-band transitions in Eq.(28), for electron doping.

$$\eta = \frac{1}{N_k} \sum_{\mathbf{k}, i, j \neq i} \frac{f(\epsilon_{i\mathbf{k}}^{(0)} - \epsilon_F^{(0)}) - f(\epsilon_{j\mathbf{k}}^{(0)} - \epsilon_F^{(0)})}{\epsilon_{i\mathbf{k}}^{(0)} - \epsilon_{j\mathbf{k}}^{(0)}} \times | \langle \psi_{j\mathbf{k}}^{(0)} | \hat{\Delta}\rho | \psi_{i\mathbf{k}}^{(0)} \rangle |^2, \quad (28)$$

where $|\psi_{i\mathbf{k}}^{(0)} \rangle$ ($i=1,2,3,4$) are the unperturbed eigenstates of $\hat{H}_{\mathbf{k}}^{(0)}$ with eigenvalues $\epsilon_{i\mathbf{k}}^{(0)}$, $\epsilon_F^{(0)}$ is the Fermi level, $f(\epsilon_{i\mathbf{k}}^{(0)} - \epsilon_F^{(0)})$ is the occupation of state i , and N_k is the number of \mathbf{k} points used in the BZ integration.

In particular, in Eq.(28) there are six contributions obtained by mixing the four unperturbed states $|\psi_{i\mathbf{k}}^{(0)} \rangle$, with $i=1,2,3$, and 4; and we label as $\eta_{i,j}$ the contribution to η given by states i and j . Within the present TB model $\eta_{1,3}$ and $\eta_{2,4}$ are exactly zero.²⁴ Contribution $\eta_{1,2}$ vanishes for $\epsilon_F > 0$ because the two states are both occupied. Therefore, for $\epsilon_F > 0$, the important contributions to η derive from $\eta_{1,4}$, $\eta_{2,3}$, and $\eta_{3,4}$, as schematically shown in Fig.14.

In Fig.15 we show η as a function of the electron doping, obtained from Eq.(28), for an electronic temperature of 300 K. Different contributions from $\eta_{1,4}$, $\eta_{2,3}$, and $\eta_{3,4}$ are also plotted. For comparison, we report $\eta(n)$ calculated with the nonperturbative TB model. Contribution $\eta_{1,4}$ as a function of doping is constant when the Fermi level is lower than the bottom of band 4, and its absolute value starts to decrease when band 4 becomes occupied due to lower availability of empty states. Contribution $\eta_{2,3}$ is minimum for zero doping, and its absolute values decreases, as a function of the electron doping, for the same reason. Contribution from $\eta_{1,4}$ is lower than contribution from $\eta_{2,3}$ due to the energy difference in the denominator of Eq.(28), which is higher for $\eta_{1,4}$. Finally, contribution $\eta_{3,4}$ vanishes for zero doping, and its absolute value increases with increasing electron doping, due

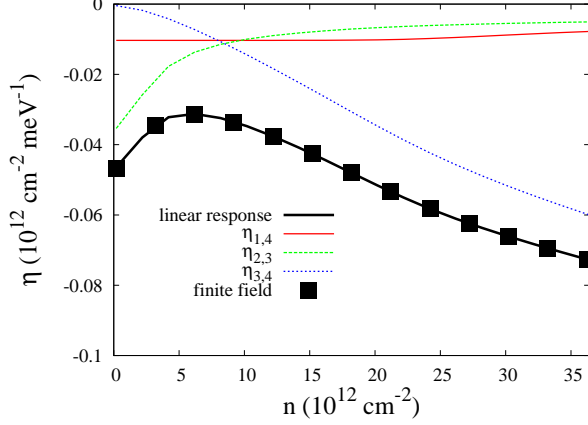


FIG. 15: (Color online) η as a function of electron doping, from Eq.(28) (linear response), and different contributions from $\eta_{1,4}$, $\eta_{2,3}$, and $\eta_{3,4}$. Squares are the nonperturbative TB results.

to larger number of possible transitions between occupied and unoccupied states.

The results in Fig.15 show that the nonmonotonic behavior of $\eta(n)$ is determined by the sum of the three contributions $\eta_{1,4}$, $\eta_{2,3}$, and $\eta_{3,4}$, which gives a maximum at the electron doping values $n \approx 6 \times 10^{12} \text{ cm}^{-2}$.

E. GW correction

Recently it has been shown by ARPES measurements that the electronic band structure of graphene and graphite is not well reproduced by LDA and GGA.²⁵ In particular, LDA and GGA underestimate the slope of the bands since these approximations do not include long-range electron-correlation effects. Such effects can fully be taken into account within the *GW* approach [where the self-energy is computed from the product of the electron Green's function (*G*) and the screened Coulomb interaction (*W*)], which is considered to be the most accurate first principles approach for the electronic band structure.²⁶ The *GW* band structures for graphite and graphene are indeed in very good agreement with the ARPES measurements.²⁷ In absence of an external electric field, the DFT-calculated bands of bilayer graphene need to be scaled in order to reproduce the *GW*-correct bands as

$$\epsilon_{i\mathbf{k}}^{GW} = \lambda \epsilon_{i\mathbf{k}}^{\text{DFT}}, \quad (29)$$

where $\lambda = 1.18$ is the scaling factor, as obtained from Ref.²⁷. Such scaling factor can change the screening properties of the bilayer, and in this section we include it in our theoretical results.

If we focus on the quantity η , we can use the perturbative expression in Eq.(28). In such expression, we

TABLE I: TB-*GW* parameters obtained by fitting the bilayer DFT bands with a TB model, along all the $\Gamma K M$ line, and by rescaling the parameters with $\lambda = 1.18$. γ_{\parallel}^i is the *i*-nearest neighbors hopping parameters. All values are in eV.

	γ_{\parallel}^1	γ_{\parallel}^2	γ_{\parallel}^3	γ_{\parallel}^4	γ_{\parallel}^5	$\gamma_{\perp}^{AA'}$	$\gamma_{\perp}^{AB'}$	$\gamma_{\perp}^{BB'}$
TB- <i>GW</i>	-3.4013	0.3292	-0.2411	0.1226	0.0898	0.3963	0.1671	0.3301

correct the DFT eigenvalues $\epsilon_{i\mathbf{k}}^{(0)}$ using Eq.(29), and we can neglect the *GW* correction to the matrix elements $\langle \psi_{j\mathbf{k}}^{(0)} | \widehat{\Delta\rho} | \psi_{i\mathbf{k}}^{(0)} \rangle$ since it is commonly found that the DFT error in the wave functions is usually negligible with respect to the error on the eigenvalues. Within this approximation, it is easy to show that

$$\eta^{GW}(\epsilon_F, T) = \frac{1}{\lambda} \eta^{\text{DFT}}\left(\frac{\epsilon_F}{\lambda}, \frac{T}{\lambda}\right), \quad (30)$$

where *T* is the temperature. The computed η^{GW} is shown in Fig.6.

α^{GW} can be computed from η^{GW} using our model in Eq.(25). In order to minimize the error from our model, we write

$$\alpha^{GW}(n) = \frac{\alpha^{\text{bare}} \beta(d - \bar{d}_a)/d}{1 - \eta^{GW}(n) \alpha^{\text{bare}} \beta(d - \bar{d}_s)/d} + \Delta, \quad (31)$$

where

$$\Delta = \alpha^{\text{DFT}} - \frac{\alpha^{\text{bare}} \beta(d - \bar{d}_a)/d}{1 - \eta^{\text{DFT}} \alpha^{\text{bare}} \beta(d - \bar{d}_s)/d}, \quad (32)$$

gives an estimate of the error in Eq.(25). The computed $\alpha^{GW}(n)$ is shown in Fig.5, and for low doping levels it is around 10% higher than the DFT value.

F. Full band structure of gated bilayer graphene

In this section we give a practical instruction to obtain the full band structure of bilayer graphene for a doping *n* and for an average electric field E_{av} . In order to do that, we fit our DFT bands along all the $\Gamma K M$ line in the BZ in absence of the external electric field, using a TB model with five nearest neighbors in-plane hopping parameters ($\gamma_{\parallel}^1, \gamma_{\parallel}^2, \gamma_{\parallel}^3, \gamma_{\parallel}^4, \gamma_{\parallel}^5$) and three out-of-plane hopping parameters ($\gamma_{\perp}^{AA'}, \gamma_{\perp}^{AB'}, \gamma_{\perp}^{BB'}$). In the Bernal stacking configuration of bilayer graphene, *A* and *A'* represent the vertically superposed atoms. These hopping parameters do not change when an external average electric field is applied. This is shown in Fig.16, where we compare the direct DFT results with the TB calculations, with the fixed hopping parameters and the *U* value from the DFT calculations.

Since we consider the *GW* one as the most precise result, in Table I we report the TB-*GW* hopping parameters obtained by fitting the DFT bands without electric field and by rescaling them with the *GW* scaling factor

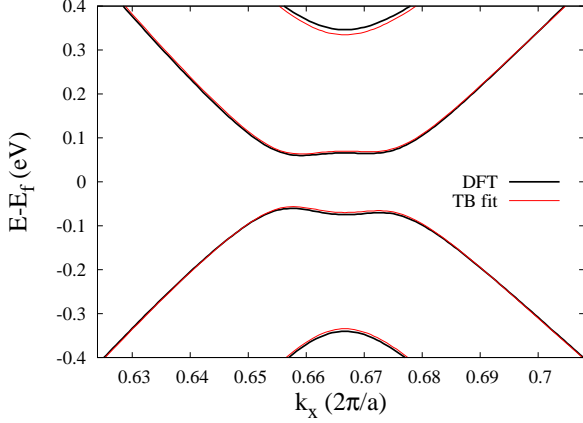


FIG. 16: (Color online) DFT-GGA calculated bands around the K point in the BZ (DFT) for $n = 0$ and with $U = 0.14$ eV and from the TB model (TB fit), with five nearest-neighbors in-plane hopping parameters and three out-of-plane hopping parameters.

TABLE II: Values of fitting parameters of Eq.(33). All values are in 10^{-12} cm^2meV .

A_1	0.896
B_1	-26.888
γ_1	21.756
A_2	3.905
B_2	1.623
γ_2	21.946
A_3	-1.654
B_3	-0.092
γ_3	5.534
C	5.848

$\lambda = 1.18$. Moreover, in order to avoid the numerical evaluation of U for a given n and E_{av} , we give a fit of our calculated $\alpha^{GW}(n)$:

$$\alpha^{GW}(n) = \sum_{i=1}^3 \frac{A_i}{\left[1 + \frac{(n - B_i)^2}{\gamma_i^2}\right]} + C, \quad (33)$$

where the values of the fitting parameters are listed in Table II. In Fig.5 we show the results of the fit with the black continuous line. From expression (33), we can obtain the value of the gap U as a function of the doping n and of the external average electric field E_{av} ,

$$U(n, E_{av}) = \alpha^{GW}(n)(n_1 - n_2), \quad (34)$$

where $(n_1 - n_2) = E_{av}/(|e|/(2\epsilon_0))$. n , n_1 , and n_2 are in units of 10^{12}cm^{-2} .

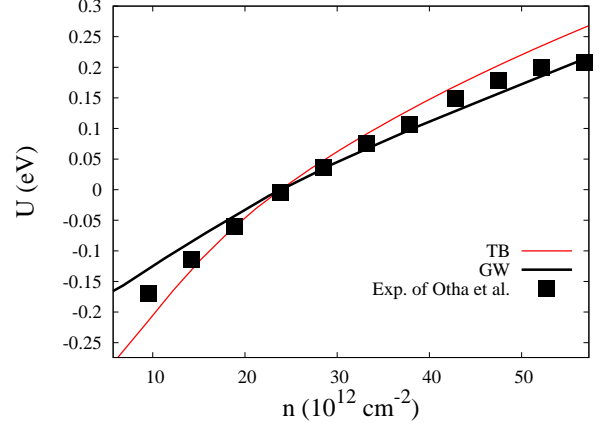


FIG. 17: (Color online) Comparison between experimental results for U from Ref.³ (squares), TB, and GW results.

G. Comparison with experimental results

In this section we compare our DFT and TB results with the direct measurement (ARPES) of the band-gap on epitaxially growth bilayer graphene in Ref.³. In this work Ohta *et al.*³ performed an experiment where bilayer graphene is synthesized on silicon carbide (SiC) substrate. The SiC acts as a fixed bottom gate, and a charge n_2 flows from the substrate to the bilayer. Further electron doping is induced with the deposition of potassium atoms on the other side of the bilayer, and this chemical doping acts as a top gate. Varying the concentration of potassium, the asymmetry between the two layers of graphene is modified, and a band-gap is opened accordingly. Using angle-resolved photoemission spectroscopy Ohta *et al.*³ directly measured the band structure, and fitting it with a TB model, they obtained a curve of the gap as a function of the doping charge in the bilayer.

To compare with their experimental results, we calculate the gap using $\alpha^{GW}(n)$ from Eqs.(33) and (34) and keep n_2 (bottom gate) fixed at $11.9 \times 10^{12}\text{cm}^{-2}$. This value of n_2 derives from the fact that in Ref.³, for a total doping of $n = 23.8 \times 10^{12}\text{cm}^{-2}$, no gap is observed, meaning that $n_1 = n_2 = n/2$. Since in the experiment the bottom gate is not varied, we also keep it fixed to this value, and we only vary $n_1 = n - n_2$.

In Fig.17 we compare our results, obtained with α^{GW} and with α^{TB} , with the experimental data from Ref.³. We first notice that the nonlinearity is not due to the saturation of the gap with E_{av} ; it is instead due to the dependence of α on the doping n (at high doping α decreases with n). Moreover, both GW and TB results are in good agreement with experiments. This is due to the fact that the experiment is carried out at high doping levels, where the difference between the GW and TB α 's is less important with respect to low doping levels (see

Fig.5).

In the case of exfoliated bilayer graphene, direct experimental measurements of the band structure and of the gap with ARPES are still unavailable. Alternatively, indirect information on the band structure can be obtained by infrared reflectivity studies. Recently, Kuzmenko *et al.*¹⁷ reported an experimental work on infrared spectra of exfoliated and gated bilayer graphene as a function of doping. In this work the authors found a strong gate-voltage dependence of their spectral features, which are related to interband transitions. A comparison of the experimental infrared spectra with the one obtained from TB calculations suggests that the TB prediction of gate-induced band-gap is overestimated.¹⁷ However, a quantitative analysis of the band-gap as a function of doping and external field is not given.

Finally, by measuring the cyclotron mass as a function of doping in bilayer graphene one can check the presence of a finite band-gap. These measurements do not provide a direct estimate of the band-gap; however, they give important informations on the hole-electron asymmetry and on the deformation of the band structure in the presence of an external electric field. In particular, in Refs.⁷ and⁸ the authors measured the cyclotron mass on exfoliated bilayer graphene. The bottom gate is realized with an oxidized silicon substrate, which allows a variation in bottom gate electron density n_2 during the experiment. The top gate is provided by chemical doping, by deposition of NH_3 molecules, which provides a top gate electron density n_1 , which is fixed during the experiment.

To compare the experimental results of Refs.⁷ and⁸ with our band structures, we calculate the cyclotron mass m_c as

$$m_c(n) = \frac{\hbar^2}{2\pi} \left(\frac{dA(E)}{dE} \right)_{E=E_f(n)}, \quad (35)$$

where A is the \mathbf{k} -space area enclosed by the orbit with energy E and E_f is the Fermi level. The derivative in Eq.(35) is obtained by finite differentiation with respect to E . For the *GW* calculations we use the band structure calculated as described in Sec. III F.

In Fig. 18 we compare the experimental data on the cyclotron mass from Ref.⁷ with our [Fig.18(a)] *GW* calculations and with [Fig.18(b)] TB calculations²⁸ for different values of top gate electron density n_1 . In Ref.⁷ the authors estimated an initial doping n_0 on bilayer graphene, at zero bottom gate, of about $1.8 \times 10^{12} \text{cm}^{-2}$. In principle, such initial doping could come both from the deposited NH_3 molecules (*i.e.*, from the top gate) and from a charge transfer from the SiO_2 substrate (*i.e.*, from the bottom gate). Thus an exact estimation of the top gate electron density n_1 is not possible, and we calculate the cyclotron mass for values of n_1 between $1.8 \times 10^{12} \text{cm}^{-2}$ and 0. Our results show that for both *GW* and TB calculations, the cyclotron mass behavior as a function of doping depends on the value of n_1 . In particular, for the

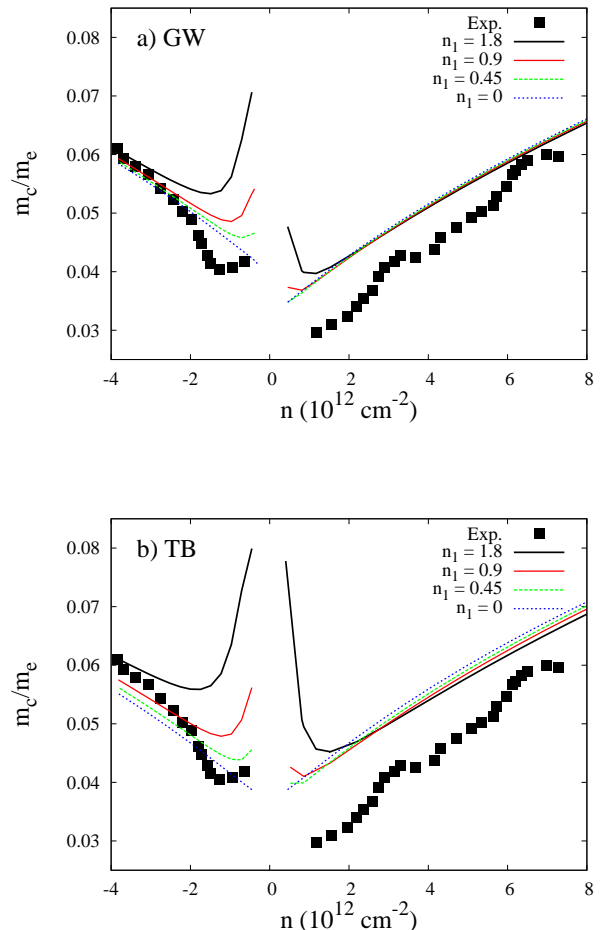


FIG. 18: (Color online) Cyclotron mass, with respect to the free electron mass m_e , as a function of doping n : comparison of the experimental results from Ref.⁷ with our (a) *GW* calculations and with our (b) TB calculations for different values of n_1 (the values of n_1 are in units of 10^{12}cm^{-2}).

GW calculations the best agreement with the experimental results is obtained for $n_1 = 0.45 \times 10^{12} \text{cm}^{-2}$. Finally, we note that our *GW* calculations give better results than the TB ones. In particular, contrary to the TB results, they are able to reproduce the hole-electron asymmetry.

IV. CONCLUSIONS

We present a detailed ab initio DFT investigation of the band-gap opening and screening effects of gated bilayer graphene. First, we analyze the response of the band-gap to the external average electric field at fixed doping. We show that this response is linear for different electron and hole doping values and for large electric field values. We then find that the linear response of the gap to the electric field has a nonmonotonic behavior as

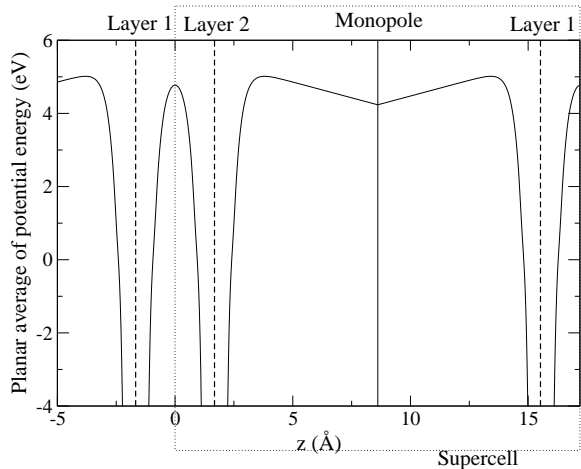


FIG. 19: Planar average of the ionic, Hartree, and monopole potentials, multiplied by the electron charge. This figure corresponds to a doping charge on the bilayer $n = 19 \times 10^{12} \text{ cm}^{-2}$. The positions of the first and second layers of the bilayer and of the monopole in the supercell are indicated.

a function of doping and for low doping values it depends on the temperature.

We also perform TB calculations for the band-gap opening. At low doping values, which are the interesting ones for electronic applications, we find that the DFT-calculated gap is roughly half of the TB one. Since the band-gap strongly depends on the screening effects, we perform a detailed analysis of the charge distribution in the bilayer in presence of the external electric field. We show that the electronic screening is characterized by interlayer and intralayer polarizations. The latter one, not included in TB calculations, gives an important contribution to the band-gap opening.

On the basis of this analysis, we propose a model which significantly improves the description of the electronic properties of bilayer graphene in the presence of an external electric field, and finally we provide a practical scheme to obtain the full band structure of gated bilayer graphene for arbitrary values of the doping and of the external electric field.

ACKNOWLEDGMENTS

Calculations were performed at the IDRIS supercomputing center (Project No. 081202 and 081387).

APPENDIX A: DIPOLE AND MONOPOLE POTENTIAL

Standard plane-wave ab initio codes work with periodically repeated super-cells. When doping the sample with

a total charge neA (A is the area of the section of the periodic cell parallel to the graphene plane) a compensating uniform background charge (with opposite sign) is added in order to have a neutral system and, thus, a periodic electrostatic potential.

In this work, we use a different approach, and we add a "monopole", that is a uniformly charged plane equidistant from the two graphene layers, with total charge $-neA$. This is done by adding in real space a periodic potential energy given by

$$V_{\text{mon}}(\bar{z}) = -\frac{ne^2}{2\epsilon_0} \left(-\bar{z} + \frac{\bar{z}^2}{L}\right), \quad (\text{A1})$$

where $\bar{z} = z - z_{\text{mon}}$, z_{mon} is the z coordinate of the monopole plane, and $\bar{z} \in [0; L]$, where L is the length of the supercell along z . While the linear term of V_{mon} is the potential associated with the monopole plane, the quadratic term cancels the potential associated with uniform background. V_{mon} can be added to the electrostatic potential acting on the Kohn-Sham electronic states with a straightforward implementation. The resulting system is, as a whole, neutral and periodic.

In Fig. 19 we show the planar average of the ionic, Hartree, and monopole potentials, multiplied by the electron charge. The position of the first and second layers of the bilayer in the supercell is indicated, together with the monopole position. The distance between the monopole and the bilayer is 6.93 \AA . This figure corresponds to a doping charge on the bilayer $n = 19 \times 10^{12} \text{ cm}^{-2}$ and to an experimental setup where the bottom and top gates are equal, and no gap opening is expected.

In order to have different bottom and top gates, we add to the monopole a sawlike potential, called dipole potential,²⁹ generated by two planes of opposite charge, as implemented in standard distributions of the PWSCF code²¹. The dipole is centered around the monopole, and the distance between the dipole planes is kept fixed to 0.17 \AA . In Fig. 20 we show the planar average of the ionic, Hartree, monopole, and dipole potentials multiplied by the electron charge for a doping charge $n = 19 \times 10^{12} \text{ cm}^{-2}$. In the case shown in the figure, the dipole potential is chosen to create a flat potential and zero electric field on layer 1 of the bilayer. This configuration corresponds to the case where only a bottom gate acts on the bilayer. By changing the sign to the dipole potential, we can obtain the opposite configuration, with a flat potential and zero electric field on layer 2 of the bilayer.

The electric fields E_1 and E_2 are calculated from the planar average of the ionic, Hartree, monopole, and dipole potential energy $V_1(z)$ and $V_2(z)$ on side 1 and side 2 of the bilayer, respectively, as

$$E_1 = -\left(\frac{1}{e}\right) \frac{dV_1(z)}{dz}, \quad (\text{A2})$$

$$E_2 = -\left(\frac{1}{e}\right) \frac{dV_2(z)}{dz}. \quad (\text{A3})$$

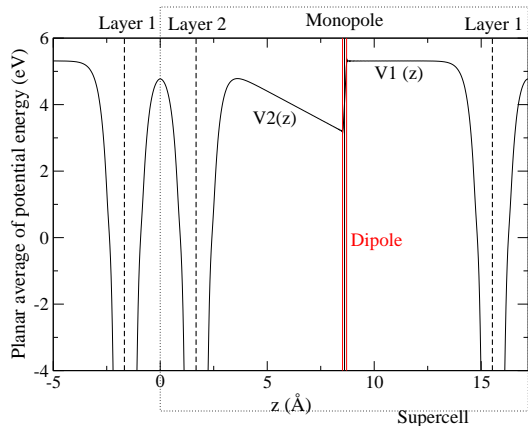


FIG. 20: Planar average of the ionic, Hartree, monopole, and dipole potentials multiplied by the electron charge. The positions of the first and second layers of the bilayer, of the monopole, and of the dipole in the supercell are indicated. This figure corresponds to a doping charge on the bilayer $n = 19 \times 10^{12} \text{ cm}^{-2}$. The dipole potential is such that layer 1 of the bilayer does not feel any external electric field.

In order to deal with uniform E_1 and E_2 electric fields, these derivatives are calculated in the linear part of $V_1(z)$ and $V_2(z)$ (see Fig.20).

Varying independently the dipole potential and the total charge on the sample and monopole, one can explore all the situations with different doping n on the bilayer and different $E_{av} = (E_1 + E_2)/2$.

- ¹ E. McCann and V. Fal'ko, Phys. Rev. Lett. **96**, 086805 (2006).
- ² F. Guinea, A. H. Castro Neto, and N. M. R. Peres, Phys. Rev. B **73**, 245426 (2006).
- ³ T. Ohta, A. Bostwick, T. Seyller, K. Horn, and E. Rotenberg, Science **313**, 951 (2006).
- ⁴ J. B. Oostinga, H. B. Heersche, X. Liu, A. F. Morpurgo, and L. M. K. Vandersypen, Nature Mater. **7**, 151 (2008).
- ⁵ E. McCann, Phys. Rev. B **74**, 161403(R) (2006).
- ⁶ H. Min, B. Sahu, S. K. Banerjee, and A. H. MacDonald, Phys. Rev. B **75**, 155115 (2007).
- ⁷ E. V. Castro, K. S. Novoselov, S. V. Morozov, N. M. R. Peres, J. M. B. Lopes dos Santos, J. Nilsson, F. Guinea, A. K. Geim, and A. H. Castro Neto, Phys. Rev. Lett. **99**, 216802 (2007).
- ⁸ E. V. Castro, K. S. Novoselov, S. V. Morozov, N. M. R. Peres, J. M. B. Lopes dos Santos, J. Nilsson, F. Guinea, A. K. Geim, and A. H. Castro Neto, arXiv:0807.3348 (unpublished).
- ⁹ M. Aoki and H. Amawashi, Solid State Commun. **142**, 123 (2007).
- ¹⁰ S. Latil and L. Henrard, Phys. Rev. Lett. **97**, 036803 (2006).
- ¹¹ R. M. Ribeiro, N. M. R. Peres, J. Courtinho, and B. P. R., Phys. Rev. B **78**, 075442 (2008).
- ¹² E. K. Yu, D. A. Stewart, and S. Tiwari, Phys. Rev. B **77**, 195406 (2008).
- ¹³ L. M. Malard, J. Nilsson, D. C. Elias, J. C. Brant, F. Plentz, E. S. Alves, A. H. Castro Neto, and M. A. Pimenta, Phys. Rev. B **76**, 201401(R) (2007).
- ¹⁴ J. Yan, E. A. Henriksen, P. Kim, and A. Pinczuk, Phys. Rev. Lett. **101**, 136804 (2008).
- ¹⁵ A. Das, B. Chakraborty, S. Piscanec, S. Pisana, A. K. Sood, and A. Ferrari, arXiv:0807.1631 (unpublished).
- ¹⁶ L. M. Malard, D. C. Elias, E. S. Alves, and M. A. Pimenta, PRL **101**, 257401 (2008).
- ¹⁷ A. B. Kuzmenko, E. van Heumen, D. van der Marel, P. Lerch, P. Blake, K. S. Novoselov, and A. K. Geim, PRB **79**, 115441 (2009).
- ¹⁸ J. P. Perdew, K. Burke, and M. Ernzerhof, Phys. Rev. Lett. **77**, 3865 (1996).
- ¹⁹ J. P. Perdew and A. Zunger, Phys. Rev. B **23**, 5048 (1981).
- ²⁰ N. Troullier and J. L. Martins, Phys. Rev. B **43**, 8861 (1991).
- ²¹ S. Baroni, A. Dal Corso, S. de Gironcoli, and P. Giannozzi, *Pwscf and phonon: plane-wave pseudopotential codes*, <http://www.pwscf.org/> (2005).
- ²² S. Baroni, A. Dal Corso, S. de Gironcoli, P. Giannozzi, C. Cavazzoni, G. Ballabio, S. Scandolo, G. Chiarotti, P. Focher, A. Pasquarello, et al., *Quantum espresso: open-source package for research in electronic structure, simulation, and optimization*, <http://www.quantum-espresso.org/> (2005).
- ²³ K. S. Novoselov, A. K. Geim, S. V. Morozov, D. Jiang, M. Katsnelson, I. Grigorieva, S. Dubonov, and A. Firsov, Nature **438**, 197 (2005).
- ²⁴ This selection rule is strictly valid for the present TB Hamiltonian, which has only the out-of-plane hopping parameter between A and A' atoms. In this case, the eigenvectors 1 and 3 of $\hat{H}_{\mathbf{k}}^0$ are four-component vectors of the form $(1, a, -1, -a^*)$. Eigenvectors 2 and 4 are of the form $(1, a, 1, a^*)$. Because of this, given the definition of $\widehat{\Delta}\rho$ [Eq.(27)], it can be easily shown that $\eta_{1,3} = 0$ and $\eta_{2,4} = 0$. For the most general Hamiltonian, $\eta_{1,3}$ and $\eta_{2,4}$ are not exactly zero but are still much smaller than the other transitions.
- ²⁵ A. Grüneis, C. Attacalite, T. Pichler, V. Zabolotnyy, H. Shiozawa, S. L. Molodtsov, D. Inosov, A. Koitzsch, M. Knupfer, J. Schiessling, et al., Phys. Rev. Lett. **100**,

037601 (2008).

- ²⁶ F. Aryasetiawan and O. Gunnarsson, Rep. Prog. Phys. **61**, 237 (1998).
- ²⁷ A. Grüneis, C. Attacalite, L. Wirtz, H. Shiozawa, R. Saito, T. Pichler, and A. Rubio, Phys. Rev. B **78**, 205425 (2008).
- ²⁸ In Refs.⁷ and⁸ the authors compared the experimental results on the cyclotron mass with TB calculations, obtained using a parameter $\gamma_{\perp} = 0.22$ eV. This value of γ_{\perp} is chosen so that theory and experiment give the same result for the cyclotron mass at $n = 3.6 \times 10^{12} \text{cm}^{-2}$. However, γ_{\perp} corresponds to the band splitting at K between the lowest occupied π band and the highest unoccupied π band (see Fig.2). γ_{\perp} can be measured with different experimental techniques,^{3,13,17} and it is found to be around 0.4 eV. Therefore, here we compare the experimental results with the cyclotron mass calculated in the TB formalism as described in Sec. II B, using $\gamma_{\perp} = 0.4$ eV, in agreement with values found in literature.
- ²⁹ B. Meyer and D. Vanderbilt, Phys. Rev. B **63**, 205426 (2001).